Geothermal resources in Egypt integrated with GIS-based analysis

Article *in* Journal of Volcanology and Geothermal Research · October 2018

DOI: 10.1016/j.jvolgeores.2018.09.013

5 authors, including:

Mohamed Abdel Zaher
National Research Institute of Astronomy and Geophysics
106 PUBLICATIONS **1,141** CITATIONS
SEE PROFILE

Samah Elbarbary
32 PUBLICATIONS **435** CITATIONS
SEE PROFILE

Hany Mesbah
National Research Institute of Astronomy and Geophysics
33 PUBLICATIONS **402** CITATIONS
SEE PROFILE

Abd-Alrahman Embaby
Damietta University
34 PUBLICATIONS **233** CITATIONS
SEE PROFILE

Contents lists available at ScienceDirect

Journal of Volcanology and Geothermal Research

journal homepage: www.elsevier.com

Geothermal resources in Egypt integrated with GIS-based analysis

M. Abdel Zaher[a, *], S. Elbarbary[a], A. El-Shahat[b], H. Mesbah[a], A. Embaby[c]

[a] National Research Institute of Astronomy and Geophysics (NRIAG), 11421 Helwan, Cairo, Egypt
[b] Geology Department, Faculty of Science, Mansoura University, 35516, Egypt
[c] Geology Department, Faculty of Science, Damietta University, 34517, Egypt

ARTICLE INFO

Article history:
Received 17 March 2018
Received in revised form 28 September 2018
Accepted 29 September 2018
Available online xxx

Keywords:
Geothermal resources
GIS
Favourability map
Red Sea - Gulf of Suez rift

ABSTRACT

The energy of Egypt is generally derived from petroleum products. However, advancements in the development of the generation capacity using sustainable and renewable resources, for example, solar, wind and geothermal resources and investment in nuclear power plants are planned. The geology and structure setting of Egypt affirms that reasonable geothermal resources are available, particularly along the Gulf of Suez, the Red Sea, the Western Desert and parts of the Nile Valley. The main objective of this research is to develop a geothermal favourability map of Egypt, which may be considered as a screening tool for the assessment of optimal areas for geothermal development. Digital data layers and maps were employed in a GIS model to select the most promising areas for geothermal potentiality. The ArcGIS model includes six thematic layers: distance to faults, Bouguer anomaly, distance to seismic activity, Curie depth, heat flow, and temperatures at different depths. The validation of the generated geothermal favourability map was performed by a comparison with thermal water wells and hot springs. Generally, the most encouraging zones for geothermal probability in Egypt are located near the shorelines of the Gulf of Suez and the Red Sea.

1. Introduction

Egypt is an electricity-poor-country, as the annual electricity production (31,600 MW) is low relative to the total population of 92 million (Al-Ahram Weekly, 2016). Because of increasing urbanization and economic development, Egypt needs to diversify its sources of energy including renewable energy side by side with other ordinary energy. Wherefore, the Egyptian Government pays more attention to renewable energy and plans to supply 20% of created electricity from renewable resources by 2022. Therefore, it is very important and urgent to use geothermal resources to generate electricity and contribute to supply Egypt's energy demands in a clean and efficient way.

Egypt has some geothermal resources with the potential for development of other renewable energy sources. An active geothermal area in Egypt indicated by geothermal surface manifestations such as thermal water wells and hot springs (Fig. 1). Many hot springs are distributed along the coasts of the Gulf of Suez (Ayun Musa 37 °C, Ain Hammam Faraun 71 °C, Hammam Musa 48 °C, and Ain Sukhna 33 °C). Some hot springs are located in the Western Desert in the Kharga, Dakhla, Bahariya and Siwa oases. These hot springs are natural indicators of heat transportation through the Earth and geothermal activity. In Egypt, geothermal waters are employed in direct heating, greenhouse cultivation, and swimming pools (Lund and Boyd, 2015; Lashin, 2015; Elbarbary et al., 2018).

The geothermal potentiality of Egypt has been investigated by many authors in different regions, such as Morgan et al. (1983, 1985), Swanberg et al. (1983), Boulos (1990), Hosney (2000), Abdel Zaher et al. (2011a, 2011b, 2012a, 2012b, 2018), Lashin (2013, 2015), Chandrasekharam et al. (2015, 2016a, 2016b), Mohamed et al. (2015), and Atef et al. (2016). GIS-based techniques have been applied in many countries, such as northern Japan (Noorollahi et al., 2007), USA (Coolbaugh et al., 2005), Iran (Yousefi et al., 2010; Noorollahi et al., 2008), and Italy (Trumpy et al., 2015, 2016), to detect geothermal resources.

This study focuses on the use of a GIS-based technique in geothermal exploration based on various sets of data, including structure geology (faults and fractures), geophysical data (aeromagnetic and aerogravity measurements and seismicity data), geothermal well data (temperature gradient and heat flow), and remote sensing data. These data sets can be combined in different evidence layers (thematic maps) using a GIS model that provides a geothermal favourability map of Egypt, which indicates the most promising prospect areas for geothermal development. The evidence layers (thematic maps) in the model are distance to faults, Bouguer, distance to seismic activity, distance to geothermal manifestations, curie depth, heat flow, and temperature distributions at different depths layers.

2. Geological and structure layers of evidence

The 1st evidence layer is derived from the geology and structural setting of Egypt, which have important roles in the distribution of geothermal resources. The spatial distribution of clastic sedimentary rocks, carbonate rocks and basement rocks were digitized from the

* Corresponding author.
Email address: moh_zaher@nriag.sci.eg (M. Abdel Zaher)

https://doi.org/10.1016/j.jvolgeores.2018.09.013
0377-0273/

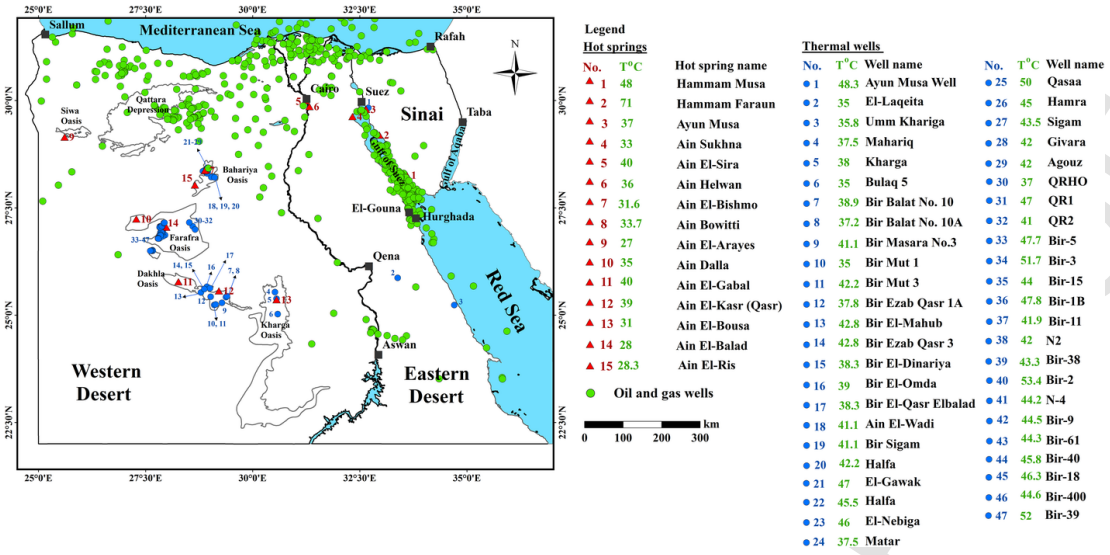

Fig. 1. Location map of the main geothermal manifestations in Egypt, including hot springs and thermal water wells. The figure shows the locations of oil and gas wells used to estimate geothermal gradients and heat flow maps of Egypt. The well data were provided by the Egyptian General Petroleum Corporation.

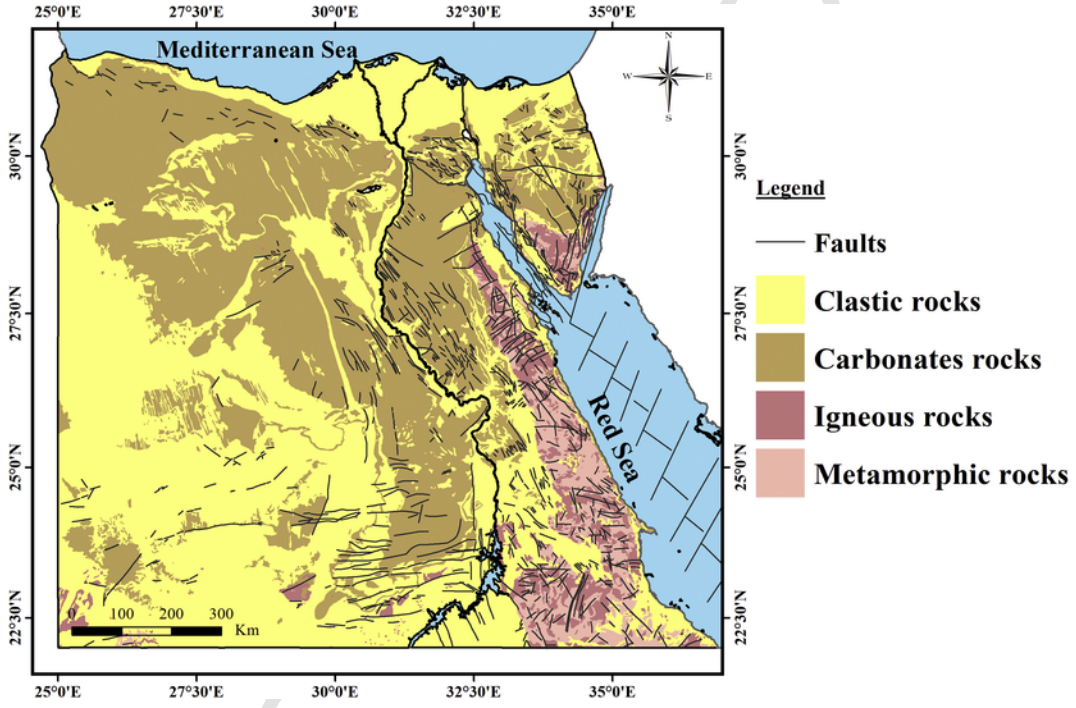

Fig. 2. Simplified geological map of Egypt, modified after a geological map of Egypt on the scale 1:2 million ©Geological Survey of Egypt (GSE, 1981). The lithological rock unites were classified into clastic sedimentary, carbonate and basement rocks based on their properties of thermal conductivity. The lines denote the structure lines (faults).

geological map of Egypt (GSE, 1981), employed as a thematic layer (Fig. 2). The Basement rocks (igneous and metamorphic) represent about 10% of Egypt surface area. Surface outcrops of the Basement rocks in Egypt are controlled by tectonism and about 90% of these rocks is buried under the Phanerozoic sedimentary cover (El-Shazly, 1977). Basement exposures are found in the eastern part of the Eastern Desert, the Nile Valley at Aswan, southern Sinai, the southeastern part of the Western Desert, and Gebel EI-Oweinat in the southwestern corner of the Western Desert.

Faults and fractures play a significant role in geothermal fields, because fluids mostly flow through fractures in the subsurface rocks (Hanano, 2000). Main faults were extracted and digitized from a geological map of Egypt (GSE, 1981) (Fig. 2). These faults enabled us to identify high permeable zones that may play a role as a pathway for the up-flow of hydrothermal fluid. They are also applied to identify the most permeable zones for well sites. Furthermore, the geothermal activity in Egypt is associated with the tectonic evolution. Northern part of Egypt is subjected to the relative movements of Africa, Arabia and Eurasia plates. Where, the Red Sea is a NW-SE trending rift initiated during Cenozoic times between the Arabian and African shields (Jarrige et al., 1990). The Red Sea and its two branches (the Gulf of

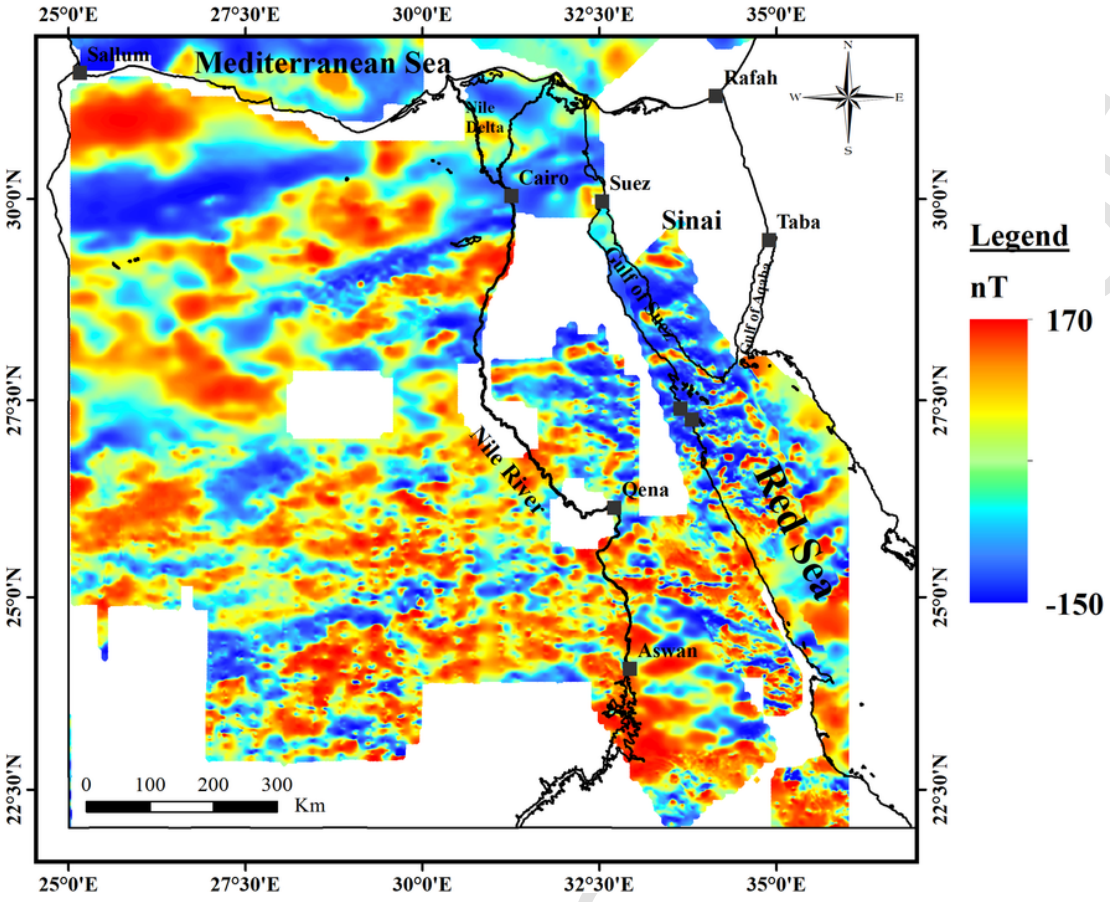

Fig. 3. Aeromagnetic map of Egypt (1 km digital grid) obtained from the "African Magnetic Mapping Project" (AMMP), (Getech, 1992; Green et al., 1992). White areas in the map are due to the lack of data in those areas not surveyed by AMMP.

Suez and Gulf of Aqaba) form the northern extension of the East African Rift (Dahy, 2012).

3. Geophysical evidence layers

3.1. Curie-depth map derived from aeromagnetic data

The airborne magnetic data are extracted from the grid of AMMP (Africa Magnetic Mapping Project). The AMMP final products contain 1 km digital grid of total field crustal anomalies at a mean terrain clearance of 1000 m produced from aeromagnetic, marine magnetic, ground measurement and Magsat data (Getech, 1992; Green et al., 1992). Some areas are not surveyed by AMMP. The total intensity aeromagnetic map of Egypt clarifies that the magnitudes of the magnetic field vary from −150 nT to +170 nT (Fig. 3).

The 2rd evidence layer comprises the Curie point depths (CPDs) of Egypt, which are the depths in the crust of the Earth where ferromagnetic minerals are converted to paramagnetic minerals due to an increase in temperature (>580 °C); a distinct magnetic field underneath is generally undetected (Hsieh et al., 2014). The Curie point depths were calculated from a radially average power spectrum by dividing the aeromagnetic map of Egypt into overlapping square sub-regions (95 windows) with dimensions of 293 × 278 km. The centroid method was applied to estimate the CPDs based on a spectral analysis of the aeromagnetic data (Okubo et al., 1985; Tanaka et al., 1999). The depths to the centroid (Z_0) and to the top (Z_t) of a magnetic layer are calculated from the slope of radially averaged power spectrum of the magnetic anomaly and then the basal depth (Z_b) can be calculated from the relation $Z_b = 2Z_0 - Z_t$ (Okubo et al., 1985). The basal depth of a magnetic source is considered to be the CPD. The estimated CPDs of Egypt range from 8.9 to approximately 35 km with an average value of 20 km (Fig. 4). The shallowest CPDs are detected in the Red Sea, whereas the deepest CPDs are detected in the Western Desert. Generally, the CPDs increase westward towards the Western Desert. CPD mapping provides information on the location of magmatic intrusions and crustal thinning at depths not accessible by other techniques. Whereas, higher temperature gradient and heat flow are expected to be associated with shallow CPDs (Okubo et al., 1985) and therefore, a higher probability of geothermal resources accessible through drilling.

3.2. Aerogravity evidence layer

The 3th evidence layer is the Bouguer map of Egypt, which comprises merged grids (onshore data accumulated from African Gravity Project (AGP) (Getech, 1992) and offshore zones taken from GETECH satellite gravity data). The gravity datum used in AGP was International Gravity Standardization Net (1971); IGSN71, theoretical gravity depends on the International Gravity Formula, IGF (1967), free air correction assumes the value 0.3086 mGal/m and the Bouguer correction reduction density is 2.67 g/cc onshore (Fairhead et al., 1988). To maintain the high resolution of GETECH satellite information (0.02 grid cell size), the AGP grids was resampled to a grid cell size of 0.02 degree and converged with satellite data. The gravity

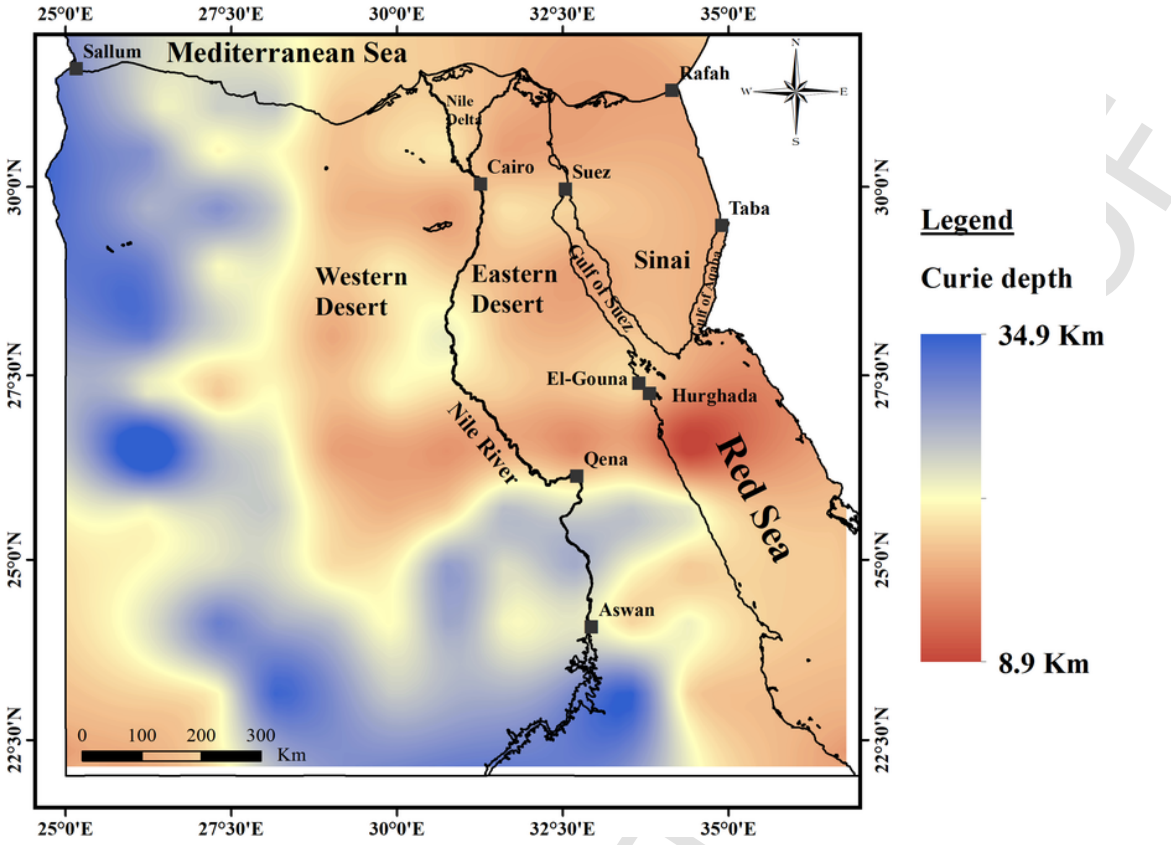

Fig. 4. Curie point depth (CPD) map of Egypt calculated from the power spectral analysis of the aeromagnetic data. The CPD is the depth in the crust of the Earth where ferromagnetic minerals are converted to paramagnetic minerals due to an increase in temperature (>580 °C).

values of Egypt range from −90.5 mgal to +126 mgal (Fig. 5). The gravity anomalies of relatively high and low amplitudes are related to density differentiation of the rocks forming the earth crust (Riad, 1977). The gravity anomaly values are positive in the Mediterranean Sea and the Red Sea, due to the effect of an oceanic region (Kovach, 1986) that causing to increase values northward and eastward of Egypt. The high gravity anomalies are expected to be related with high density basement rocks exposed in a structural high, whereas low gravity anomalies are associated to the lighter the sedimentary cover. This indicates that the source of both the high gravity anomaly and the high geothermal potentiality is thinning of the crust due to intensive structure.

3.3. Seismicity evidence layer

The 4th evidence layer consists of seismological data collected from the Egyptian National Seismic Network (ENSN) in the NRIAG for the period 1997 to 2014, which are classified based on the magnitude variation (Fig. 6). Numerous geothermal zones are consistent with regional tectonics (Foulger, 1982), that's why they display higher background seismicity than their encompassing regions. Therefore, collecting seismic events can give valuable information about a geothermal area on different scales. Extensive earthquakes have collected at the southern end of the Gulf of Suez, where the Sinai triple intersection (Africa, Arabia, and Sinai) is located (Korrat et al., 2006; Badawy and Horvath, 1999). Seismic epicenters in the Red Sea define an active zone extending S-SE from the Gulf of Suez into the axial region of the Red Sea down to 25.75°N, with micro-seismicity between 24° and 25°N, reflecting active median spreading in the northern Red Sea (Daggett et al., 1986). The Red Sea, Gulf of Suez, Gulf of Aqaba and Cairo-Suez district are the most seismically active zones in Egypt (Fig. 6). The high seismic activity in Cairo-Suez district is related to the movement of African, Eurasian and Arabian plates (Meshref, 1990). The seismic activities in the Gulf of Suez have a NW-SE trend coinciding with the main trend of the rift opening and the activity decreases from south to north (Dahy, 2012).

4. Geothermal data (thermal evidence layers)

The 4th and 5th evidence layers consist of temperature distribution at various depths and heat flow map of Egypt which depend on bottom-hole temperature (BHT) data from 596 deep onshore and offshore oil and gas wells (Fig. 1), with depths that range from 612 to 6405 m, drilled by oil companies that include the Egyptian General Petroleum Company (EGPC), the Gulf of Suez Petroleum Company (GUPCO), and the British Petroleum Company (BPC).

4.1. Bottom-hole temperature evidence layer

The real temperature is always higher than the measured temperature (BHT) from borehole logs. A large quantity of mud is circulated in the borehole during drilling to facilitate the drilling, stabilize the borehole and evacuate the cuttings. Mud circulation, duration of drilling, thermal properties of drilling fluid, and nature of heat exchange between the formation and borehole fluid give non-equilibrium temperature at the time of temperature measurements (Nwankwo and Ekine, 2009). A method for correcting log-derived temperatures (BHT) has been presented by Waples et al. (2004) in

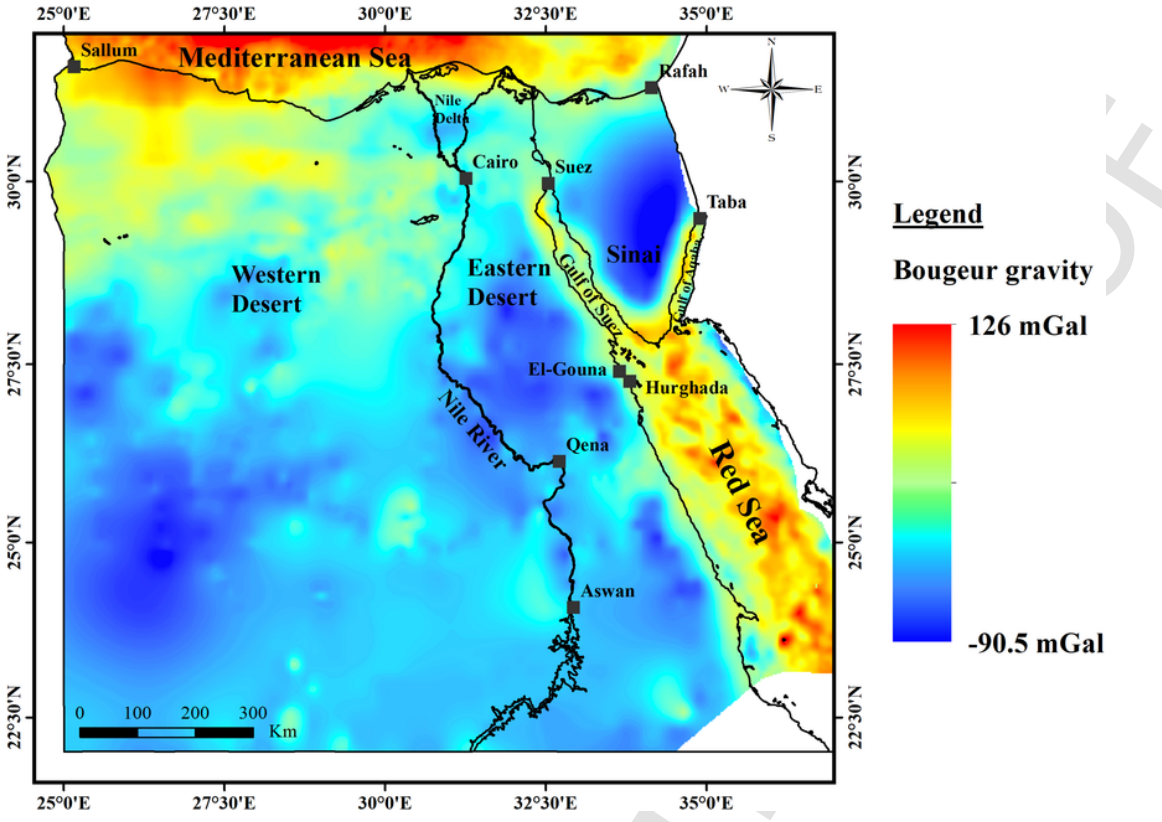

Fig. 5. Bouguer anomaly map of Egypt consists of merged grids of onshore data obtained from AGP compilation (Getech, 1992) and offshore areas taken from GETECH satellite Bouguer data. The merged data were resampled to 0.02 degree grid cell size and gridded using a minimum curvature technique.

deep wells (3500–6500 m) by the comparison between log temperatures from the Gulf of Mexico and Drill-Stem Test (DST) temperatures in the same wells. The equations are modified slightly from those of Waples and Ramly (2001), which were calibrated using data from depths <3500 m in Malaysia. The correction depends mostly on time since end of mud circulation (TSC) and depth of logging. The true subsurface temperature in Celsius is given by:

$$T_{True} = T_{Surface} + f\ (T_{meas} - T_{Surface}) - 0.001391\,(Z - 4498)$$

where $T_{surface}$ is the seafloor or land-surface temperature (°C), T_{meas} is the measured log temperature BHT (°C), TSC is in hours and Z is depth below in meters. The correction factor, f, is a function of TSC and equals:

$$f = \frac{[-0.1462 \ln\ (TSC) + 1.699]}{0.572 \times Z^{0.075}}$$

Other correction method, proposed by Horner (1951) was applied on the BHT data for confirming the corrections from Waples equation. The Horner (1951) plot method was widely used for obtaining the true formation temperature from BHT measurements. The Horner's method is based on an observed similarity in the behavior of in situ temperature and pressure when disturbed by drilling. The method was originally devised to correct pressure build-up data from drill stem tests (Horner, 1951), but was adopted for temperature correction by Lachenbruch and Brewer (1959). It involves the plot of the measured temperature T_{BHT} (at a given depth) from many logging runs against ln [1+(tc/Δt)], where Δt is the time elapsed between end of fluid circulation and measurement of T_{BHT}, and tc is the time elapsed between end of drilling and end of fluid circulation. A straight line of best fit through all points yields the true formation temperature at the T_{BHT}-axis intercept. It is recommended to use Horner method if there are three or more self-consistent BHT from a given well. In this present study, the two above methods were applied on all BHT data. Table 1 shows examples of corrected temperature by using the methods of Waples et al. (2004) and Horner (1951). Fig. 7 illustrates examples of Horner's plot for correction of BHT in four wells. The true formation temperature data were subsequently employed to estimate the temperature gradient and heat flow maps of Egypt.

Thereafter, the corrected BHT at various depths (>1000, 1000–2000, 2000–3000, <3000 m) were mapped in order to show the variation of temperatures with depths (Fig. 8). The maps show that the temperature increases with depth and reach up to 180 °C at 3000 m or more. High temperature was encountered at eastern part of Egypt in Gulf of Suez and Red Sea region. These maps were used as input layers for calculating the favourability geothermal map of Egypt.

4.2. Heat flow evidence layer

The heat flow map of Egypt was calculated by combining sets of calculated temperature gradients and the average thermal conductivity of the rocks for each well. The temperature gradient defined as the

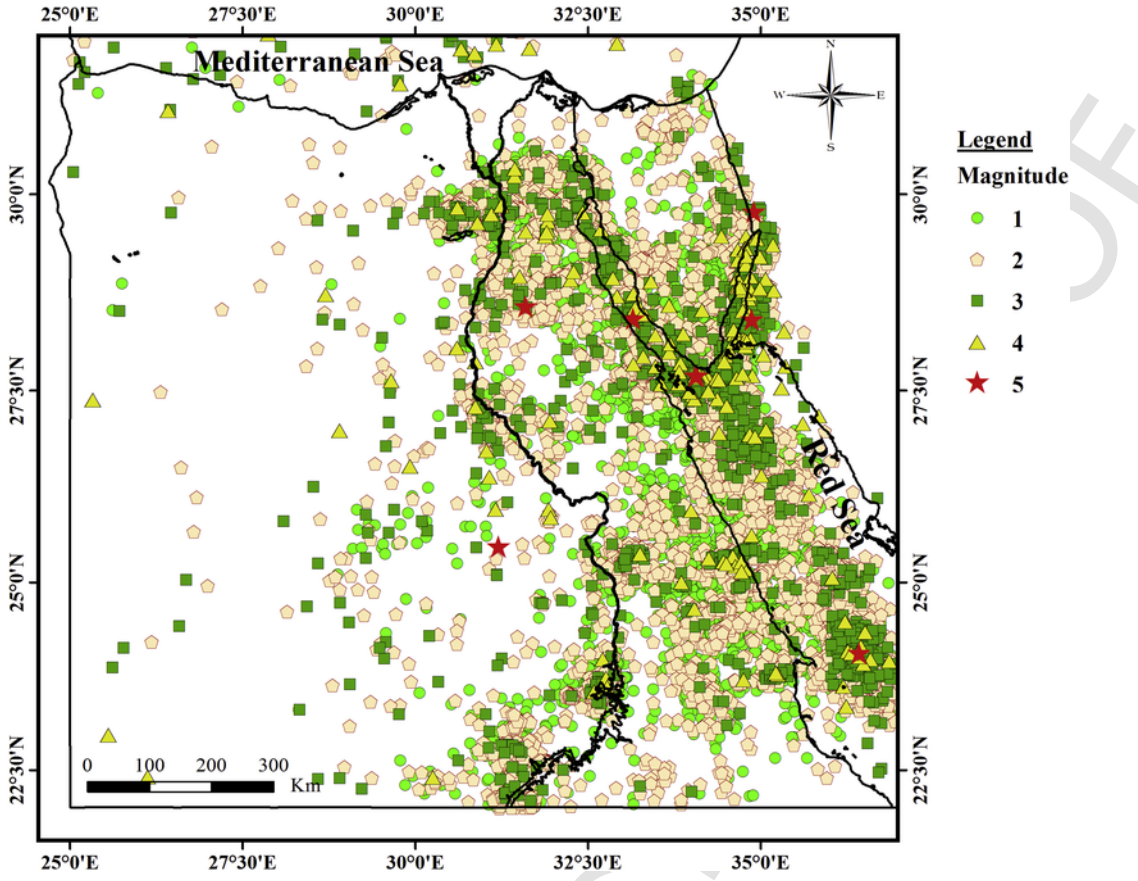

Fig. 6. Distributions of earthquake epicentral in Egypt with magnitudes that range from one to five (modified after ENSN, 2014). Most of records are concentrated in the eastern part of Egypt especially in the areas of the Gulf of Suez and Gulf of Aqaba. Distance to seismic activity was used as evidence layer for constructing geothermal favourability map of Egypt.

rate of change in temperature with respect to the depth of the well logs. It can be determined using the following equation:

$$\text{Geothermal gradient } (GG) = \frac{T_{BHT} - T_{Surface}}{Z} \times 1000$$

where GG is geothermal gradient in °C/m, T_{BHT} is the corrected temperature (BHT), $T_{surface}$ is the mean annual surface temperature, assuming of 26.7 °C (Morgan et al., 1983), and Z is the depth of measurement.

The calculated geothermal gradients in most parts of Egypt fall within the interval of 17.6 to 75 °C/km. The average value is about 31 °C/km which is closer to the world average (30 °C/km). On the other hand, thermal conductivities of bottom formation in each well was calculated based on data from Morgan et al. (1983, 1985) and information about type of bottom formation; 3.2 ± 0.1 W/m °C for basement rocks; 2.4 ± 0.2 W/m °C for sandstone; 2.2 ± 0.2 W/m °C for carbonate rocks.

The calculated heat flow map shows that heat flow values range from 26.9 to about 187 mW m^2 (Fig. 9) with an average of about 78.5 mW/m^2. The average heat flow in continental regions is approximately 62 mW/m^2. Values in excess of 80–100 mW/m^2 indicate anomalous subsurface geothermal conditions (Brott et al., 1976). The heat flow values are relatively high in the eastern parts compared to the western parts of Egypt. Although, the heat flow of most areas are in the global average, there are some hot spots with significantly higher temperature gradients. These areas are usually associated with the Red Sea-Gulf of Suez rift, around Hammam Faraun hot spring in the east of Gulf of Suez, and in El-Gouna area in the west of Gulf of Suez. There is also a high anomaly at the south of Aswan. This area is characterized by the presence of active seismic epicenters and faults. The maximum heat flow values are recorded in the Red Sea.

5. Data integration and favourability analysis

The generation of a geothermal favourability map of Egypt involves many steps. The first step is the identification of the main parameters that affect the geothermal favourability and the data collection for each parameter. In the second step, the thematic layer of each parameter is prepared, and all layers are ensured to have the same coordinate system (World Mercator WGS84). Six thematic layers are prepared: distance to faults, Bouguer anomaly, distance to seismic activity, Curie point depth, heat flow, and temperatures at different depths. These layers are the inputs of ArcGIS model builder 10.3. The third step entails reclassifying all thematic layers (Rasters) to a common favourability scale using the reclassify tool in ArcGIS 10.3. Each layer is classified using a scale (from one to nine) in which higher values are more suitable (Table 2). The favourability scores depend on the threshold values of each parameter. For the distance layers (distance to seismic activity and distance to faults), the greater is the distance from the seismic activity and faults, the lesser is the geothermal influence, and a lower value is obtained. We assumed that the earthquakes recorded are largely confined to <100 km^2 in area, so

Table 1
Results of some BHT and corrected formation temperature after Appling Horner method (1951) and Waples et al. method (2004). *Examples using the Horner (1951) method were shown in Fig. 9.

Well name	Depth (*m)	$BHT_{measured}$ (°C)	$T_{corrected}$ (°C) Horner method (1951)	$T_{corrected}$ (°C) Waples method (2004)
El-Fayrouz NE-1	2651	99.0	122.1	116.1
Drak-1	3230	110.0	129.4	128.4
Wadi Habib-1X	2281	76.7	94.1	97.6
Nagel-1	4213	109.0	114.5	115.8
1.BRE-3.1	3295	101.7	109.5	114.9
WBS-1	2072	77.8	88.6	93.6
WBS-2	2040	87.8	94.9	96.2
Halfaya-1	3602	107.2	115.5	126.1
SW Wadi Rayan-1X	1964	71.1	81.6	82.3
NB-42-1	2151	71.1	86.9	84.4
Nuqra-1	2552	86.7	103.0	101.1
EDX-1	2124	76.7	84.5	90.7
Burulus-1	2539	72.7	89.5	86.2
Bardawil-1	4130	130.0	153.4	150.7
Birigat 1	3466	88.9	96.9	99.6
Goliath-1	3201	100.6	126.8	118.2
Kabrit-1	2925	90.0	104.2	107.5
Mallaha 1X	3368	101.7	115.9	119.8
*RBOZ 108-1	1743	72.2	87.9	88.2
Raad-1	1307	63.0	81.2	81.1
PFM SE-2	3803	112.2	131.9	130.5
Tida-1	2825	87.8	100.1	99.3
Tarif-2A	4168	122.2	135.5	136.7
Ubur-1	3120	73.9	85.5	84.2
EDX-1	1819	76.7	86.3	91.8
Ashrafi West	2047	90.0	116.2	119.9
SG-300	2989	97.8	117.2	118.3
GG-83	2177	80.0	101.3	100.5
SB-268	4450	112.8	133.3	132.0
Shukeir Bay-2	2226	72.2	108.1	97.5
GS-197	3869	107.2	123.2	124.9
GS-315	3952	126.7	155.6	155.4
Darag-1	2963	98.9	121.2	115.7
GG-83-3	2619	84.4	97.7	102.2
HH-83	2060	76.1	104.2	100.1
QQ-90	2993	86.1	114.6	105.6
QQ-89	1695	58.3	67.8	73.3
FF-83	2572	91.1	110.0	108.7
*GS-346	3033	100.6	121.0	116.5
GS-326	2154	76.7	107.1	97.6
GS-316	3825	104.4	127.6	130.1
GG-85	4480	128.3	144.8	145.2
C4-S4	2966	98.9	116.5	126.1
*GS-327	2542	96.7	121.2	115.1
SB-296	3224	103.3	130.8	128.6
*C4-N4	3285	121.1	138.6	131.4
Fesyan-B-1X	1629	64.4	74.3	79.4
N. Darag-2	1579	65.0	95.6	90.1
N. Darag-3	1470	59.4	77.9	79.1
W. Gebel Zeit-2	2187	91.1	116.3	110.7
AS-404C	1874	84.0	106.8	105.4

the area <10 km from the seismic activity is assumed to be near a favourable geothermal area and is given the highest value of nine. These areas were defined as probable geothermal prospects. For the Bouguer layer, the higher is the value, the stronger is the relationship with the geothermal resources, and a higher value is assigned. For the heat flow layer, the higher are the values, the greater is the possibility of a geothermal area and the higher is the value of the favourability class. Conversely, for the Curie point depths (CPDs), the shallow depths reflect a high possibility for a geothermal area and a high value of the assigned favourability class.

A weighted overlay analysis (weight and combine layers) of thematic layers was performed using a weight overlay tool in ArcGIS 10.3 after the percentage of influence of each thematic layer on the geothermal favourability model. Fig. 10 shows a workflow diagram of the data input and the steps in the determination of the geothermal favourability of Egypt. According to the different influences of the thematic layers of geothermal favourability, each layer has a weight according to its importance in the weighed overlay model using ArcGIS 10.3.

The corrected BHTs and heat flow are the main indicators that are applied to identify the geothermal areas as they depend on real BHTs from drilled wells in Egypt. Therefore, the heat flow is given the maximum influence of 30% while the BHTs are given 20%. The strong correlation between geothermal occurrences and faults development and seismic activity are attributed to an influence of 20% for each layer. The Bouguer gravity, Curie point depth are assigned an influence of 5% for each layer. They have the least influence as they depend on estimated data from geophysical tools.

The weighted overlay of all evidence layers in this study will generate a raster file with a range of values. Higher values represent a larger number of geothermal suitable areas, whereas lower values refer to less suitable areas. The geothermal favourability map is created and reclassified to the desired favourability scale. The final favourability map is an initial screening tool for identifying potentially undiscovered geothermal resources in Egypt. The generated map is classified into five classes to select the most encouraging zones for geothermal evolution (Fig. 11).

6. Discussion

The geothermal favourability map of Egypt identifies potentially geothermal resources and suggests that it increases towards the Red Sea, Gulf of Suez rift. This finding is consistent with the results of other studies (Martinez and Cochran, 1989), which indicate that the heat flow increases seaward of the coasts to average values >250 mW/m^2 in the axial depression of the rift. The most promising areas for geothermal potentiality in Egypt in the Red Sea, at El-Gouna area along the Red Sea coast, and at Hammam Faraun (eastern coast of Gulf of Suez). The results from the favourability map require validation with ground-level data and a field study in a subsequent stage such as geochemical sampling, geophysical land surveys and updated information on geothermal manifestations. Thus, the results from a favourability map are not final and should be updated as new data become available. Selecting suitable geothermal exploration sites is the main objective of this paper. Thus, surface geothermal manifestations (hot springs and thermal water wells) are needed to verify the constructed GIS model.

The validation of the generated geothermal favourability map (Fig. 11) is performed by comparing with the hot springs and thermal water wells. The results clarify that superficial thermal manifestations (hot springs), including Ayun Musa, Ain Hammam Faraun, Hammam Musa, and Ain Sukhna, are located in the high geothermal favourability class. Other thermal wells and springs are located in the moderate geothermal favourability class. The most promising onshore geothermal areas are located in the western shore of the Red Sea and Gulf of Suez. The El-Gouna area, which is located south of the Gulf of Suez, yields higher geothermal potentiality, which may be related to the Sinai triple junction among Africa, Arabia, and Sinai. A geothermal exploration of the El-Gouna area is recommended to estimate its energy potential.

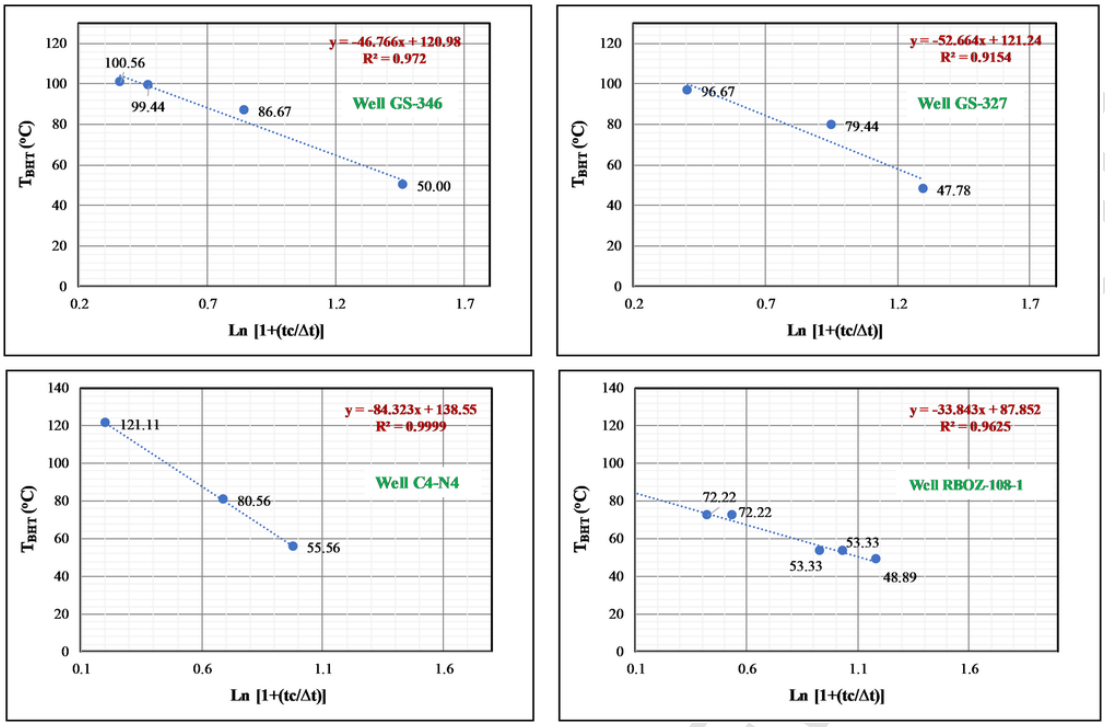

Fig. 7. Examples of the correction of bottom hole temperatures (BHT) using the Horner (1951) method. The true formation temperature was computed from the intersection of the straight line of best fit through all points with the BHT-axis. The results were listed in Table 1.

The geothermal resources in Egypt that belong to moderate-to-low-favourable geothermal areas could be suitable for direct-use applications, such as district heating and cooling, greenhouses, fisheries, mineral recovery, and industrial process heating. Aided by modern technology, even moderate temperature resources are being employed for the generation of electricity using the binary-cycle method (Gupta and Roy, 2007). The main result of this study is the implementation of the first geothermal favourability map of Egypt highlighting potentially undiscovered geothermal resources, which guide investors interested in the geothermal energy industry for planning and developing geothermal energy resources. Finally, the use of GIS-based technologies represents a helpful new strategy for predicting potentiality geothermal areas and the outcomes can be updated as new data become available.

7. Conclusions

The demand for energy in Egypt is rapidly increasing due to the increasing population and economic growth. Digital data layers and maps were employed in a GIS model to select the most promising areas for geothermal utilisation. The ArcGIS model includes six thematic layers; distance to faults, Bouguer gravity anomaly, distance to seismic activity, Curie point depth, heat flow, and temperatures at different depths. These layers were overlain by a weighted overlay analysis in a GIS, and suitable areas for geothermal exploration were defined and prioritized to generate a geothermal favourability map of Egypt. From the resultant map, a high class of geothermal favourable areas is associated with geothermal manifestations, such as Ayun Musa, Hammam Faraun and Hammam Musa, on the eastern coast of the Gulf of Suez and Ain Sukhna on its western coast. Generally, the most promising areas for geothermal potential in Egypt are near the coasts of the Red Sea and the Gulf of Suez. The El-Gouna region, which is located south of the Gulf of Suez, yields a higher geothermal probability, which may be identified with the Sinai triple intersection of Africa, Arabia, and Sinai.

Acknowledgements

The authors appreciate the support of the Egyptian *General Petroleum* Corporation (EGPC), who provided temperature data for oil and gas wells in Egypt; the Getech Group PLC., who provided airborne gravity and magnetic data; and the Egyptian National Seismic Network (ENSN) at the National Research Institute of Astronomy and Geophysics, who provided seismicity data. The authors thank Mr. Salah Khaled, Mr. Khairy Abdel-Mohsen and Mr. Mahmoud Ibrahem at EGPC and Prof. Elsayed Abdelrahman at Geophysics Dept., Cairo University, Egypt for their assistance. This study was primarily financed by a PhD grant from the Academy of Scientific Research and Technology (ASRT), Egypt.

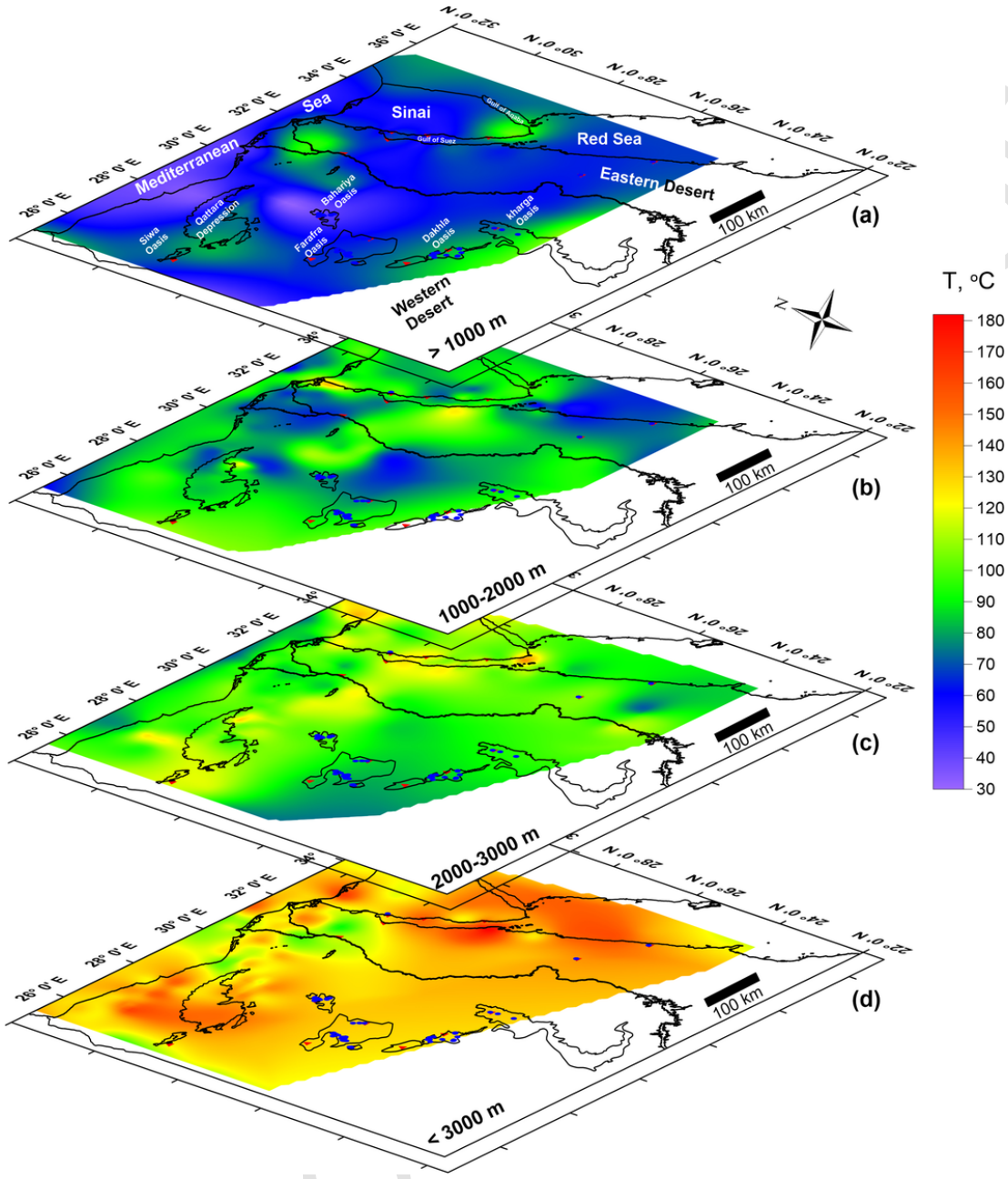

Fig. 8. The distribution of temperatures at different depths, based on the corrected BHTs from oil and gas wells, (a) depths <1000 m, (b) depths 1000–2000 m, (c) depths 2000–3000 m, and (d) depths >3000 m.

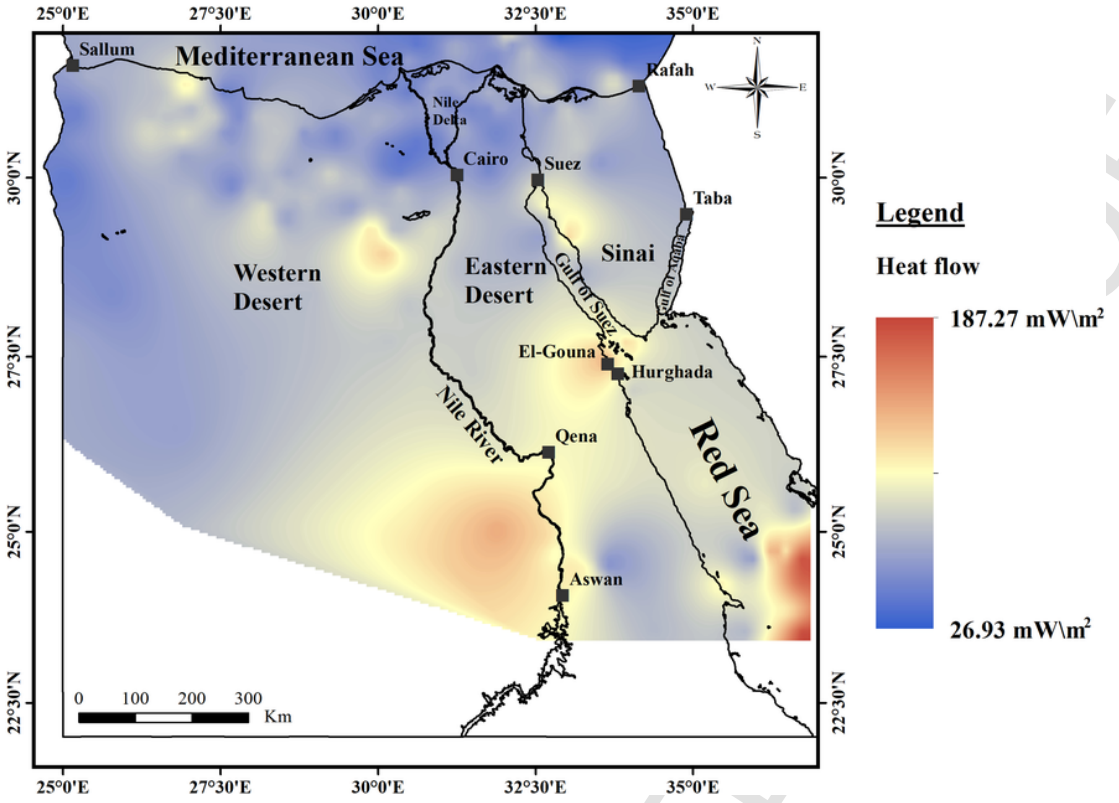

Fig. 9. Heat flow map of Egypt based on a combination of temperature data from 596 deep onshore and offshore wells, which was provided by the Egyptian General Petroleum Corporation and thermal conductivity of the rocks (average of 2.65 W/m °C) (Morgan et al., 1983, 1985). The map indicates that heat flow increases eastward of Egypt towards Red Sea and Gulf of Suez regions.

Table 2
Geothermal suitability classes for threshold variables of different thematic layers. Each layer is classified on a scale from 1 to 9; higher values are more suitable.

		Class value								
Thematic layers		1 Low	2	3	4	5	6	7	8	9 High
Geological data	Distance from faults (km)	>10	–	–	–	–	–	–	–	<10
Geophysical data	Aerogravity data Bouguer (mGal)	−90–−56	−56–−42	−42–−28	−28–−14	−14–2	2–19	19–39	39–63	63–125
	Distance from seismic activity(km)	>10	–	–	–	–	–	–	–	<10
	CPD (km)	27–35	25–27	23–25	21–23	19–21	17–19	16–17	13–16	8–13
Well data	BHT at different depths (°C)	30–40	40–50	50–70	70–90	90–110	110–130	130–150	150–170	>170
	Heat flow (mW/m^2)	26–50	50–70	70–90	90–100	100–110	110–120	120–130	130–150	150–187

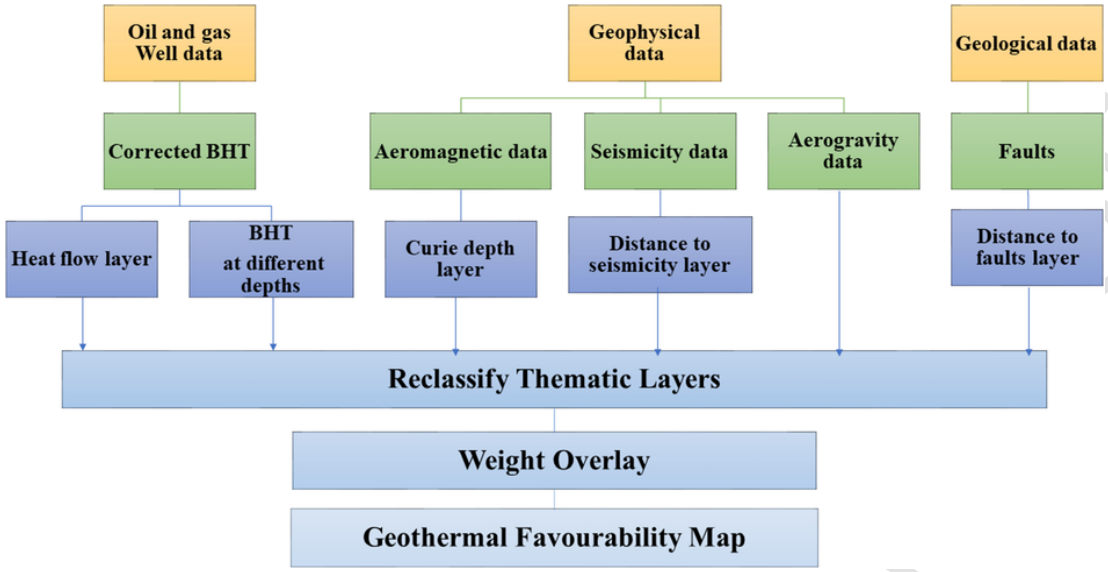

Fig. 10. Flow chart of the methodology employed to generate a geothermal favourability map of Egypt.

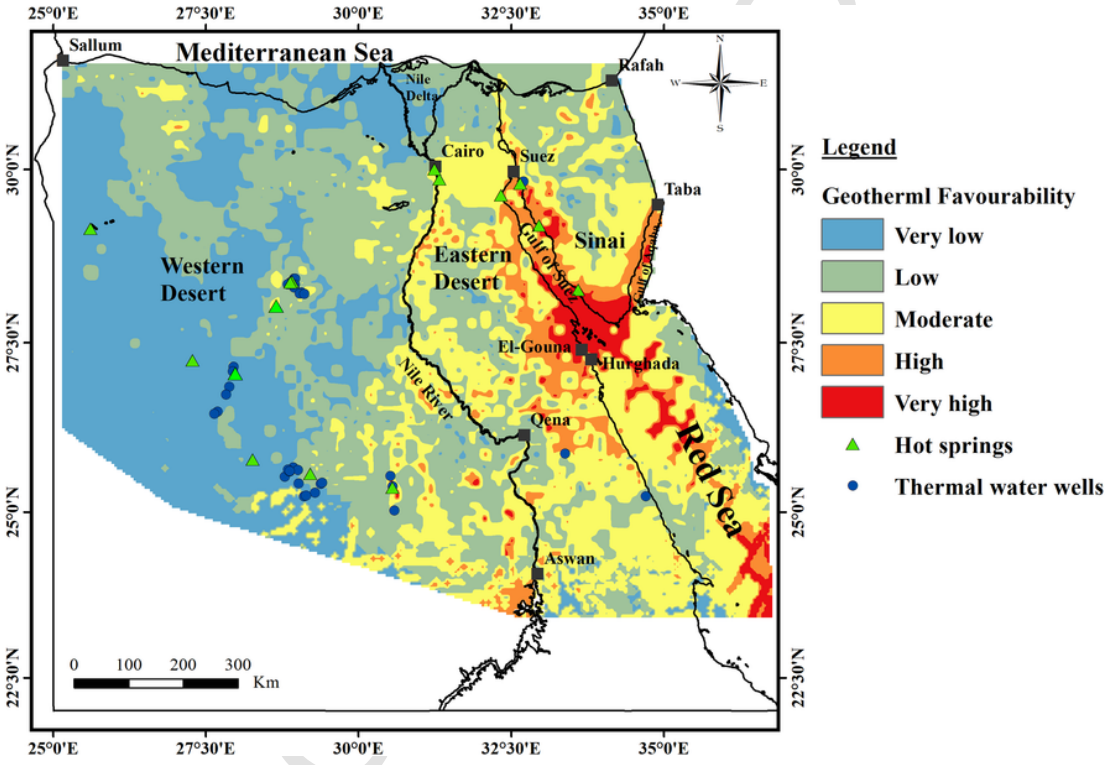

Fig. 11. Geothermal favourability map of Egypt derived from weight overlay analyses of thematic layers using the weight overlay tool in ArcGIS 10.3 after the percentage of influence of each thematic layer on the geothermal favourability model. The figure reveals that the Gulf of Suez and Red Sea represent the most encouraging zones for geothermal development.

References

Abdel Zaher, M., Saibi, H., El-Nouby, M., Ghamry, E., Ehara, S., 2011. A preliminary regional geothermal assessment of the Gulf of Suez, Egypt. J. Afr. Earth Sci. 60, 117–132.

Abdel Zaher, M., Nishijima, J., El-Qady, G., Aboud, E., Masoud, O., Soliman, M., Ehara, S., 2011. Gravity and magnetotelluric investigations to elicit the origin of Hammam Faraun hot spring, Sinai Peninsula, Egypt. J. Acta Geophys. 59 (3), 633–656.

Abdel Zaher, M., Saibi, H., Nishijima, J., Fujimitsu, Y., Mesbah, H., Ehara, S., 2012. Exploration and assessment of the geothermal resources in the Hammam Faraun hot spring, Sinai Peninsula, Egypt. J. Asian Earth Sci. 45, 256–267.

Abdel Zaher, M., Saibi, H., Ehara, S., 2012. Geochemical and stable isotopic studies of Gulf of Suez's hot springs, Egypt. Chin. J. Geochem. 31 (2), 120–127.

Abdel Zaher, M., Saibi, H., Mansour, K., Khalil, A., Soliman, M., 2018. Geothermal exploration using airborne gravity and magnetic data at Siwa Oasis, Western Desert, Egypt. Renew. Sust. Energ. Rev. 82 (3), 3824–3832.

Al-Ahram Weekly, 2016. Solar Energy and Industrial Development in Egypt. Issue 1303, (14–20 July 2016). http://weekly.ahram.org.eg/News/16790.aspx.
Atef, H., Abd El-Gawad, A., Abdel Zaher, M., Farag, K., 2016. The contribution of gravity method in geothermal exploration of southern part of the Gulf of Suez-Sinai region, Egypt. NRIAG J. Astron. Geophys. 5, 173–185.
Badawy, A., Horvath, F., 1999. Recent stress field of the Sinai subplate region. Tectonophysics 304, 385–403.
Boulos, F.K., 1990. Some aspects of the geophysical regime of Egypt in relation to heat flow, groundwater and microearthquakes. In: Said, R. (Ed.), The Geology of Egypt. Balkema, Rotterdam, pp. 61–89.
Brott, C.A., Blackwell, D.D., Mitchell, J.C., 1976. Geothermal Investigation in Idaho, Part 8, Heat Flow in the Snake River Plain Region, Idaho. 30, Department of Water Resources, Water Information Bulletin, (195p).
Chandrasekharam, D., Lashin, A., Al-Arifi, N., Al-Bassam, A., Varun, C., 2015. Evolution of geothermal systems around the Red Sea. Environ. Earth Sci. 73 (8), 4215–4236.
Chandrasekharam, D., Lashin, A., Al-Arifi, N., Al-Bassam, A., 2016. Red Sea Geothermal Provinces, Taylor and Francis Group, London, UK, (216p).
Chandrasekharam, D., Lashin, A., Al-Arifi, N., Al-Bassam, A., Varun, C., Singh, H.K., 2016. Geothermal energy potential of Eastern Desert region, Egypt. Environ. Earth Sci. 75, 697–713.
Coolbaugh, M.F., Zehner, R.E., Raines, G.L., Oppliger, G.L., Kreemer, C., 2005. Regional prediction of geothermal systems in the Great Basin, USA using weights of evidence and logistic regression in a Geographic Information System (GIS). In: Cheng, Q., Bonham-Carter, G. (Eds.), GIS and Spatial Analysis, International Association of Mathematical Geology Annual Conference Proceedings. Toronto, Canada, pp. 505–510.
Daggett, P.H., Morgan, P., Boulos, F.K., Hennin, S.F., El-Sherif, A.A., El-Sayed, A.A., Basta, N.Z., Melek, Y.S., 1986. Seismicity and active tectonics of the Egyptian Red Sea margin and the northern Red Sea. Tectonophysics 125, 313–324.
Dahy, S.A., 2012. Seismic active zones and mechanism of earthquakes in northern Egypt. Eur. J. Appl. Sci. 4 (2), 65–71.
Elbarbary, S., Abdel Zaher, M., Mesbah, H., El-Shahat, A., Embaby, A., 2018. Curie point depth, heat flow and geothermal gradient maps of Egypt deduced from aeromagnetic data. Renew. Sust. Energ. Rev. 91, 620–629.
El-Shazly, E.M., 1977. The geology of the Egyptian region. In: Nairn, A.E., Kanes, W.H., Stehli, F.G. (Eds.), The Ocean Basins and Margins. Volume 4A the Eastern Mediterranean. Plenum Press, New York, (503p).
ENSN, 2014. Egyptian National Seismological Network. Annual Seismological Bulletin. National Research Institute of Astronomy and Geophysics, Cairo, Egypt.
Fairhead, J.D., Watts, A.B., Chevalier, P., El-Haddadeh, B., Green, C.M., Stuart, G.W., Whaler, K.A., Whindle, I., 1988. African Gravity Project. Technical Report. University of Leeds Industrial Services Ltd., United Kingdom, (Unpublished report).
Foulger, G., 1982. Geothermal exploration and reservoir monitoring using earthquakes and the passive seismic method. Geothermics 11 (4), 259–268, (1982).
Getech, 1992. The African Magnetic Mapping Project. Commercial Report, (unpublished).
Green, C.M., Barritt, S.D., Fairhead, J.D., Misener, D.J., 1992. The African magnetic mapping project. Extended abstract. In: European Association of Geoscientists and Engineers (EAGE) 54th Meet Technical Exhibition, Paris.
GSE, 1981. Geological Survey of Egypt. Geologic Map of Egypt, Scale 1,2000000.
Gupta, H., Roy, S., 2007. Geothermal Energy, An Alternative Resource for the 21st Century. Elsevier, Amsterdam, The Netherlands, (279p).
Hanano, M., 2000. Two different roles of fractures in geothermal development. In: Proceedings of the World Geothermal Congress, Kyushu-Tohoku, Japan. pp. 2597–2602.
Horner, D.R., 1951. Pressure build-up in wells. In: Proceedings Third World Petroleum Congress, The Hague. p. 503.
Hosney, H.M., 2000. Geophysical Parameters and Crustal Temperatures Characterizing Tectonic and Heat Flow Provinces of Egypt. ICEHM2000 Cairo University, Egypt, 152–166.
Hsieh, H., Chen, C., Lin, P., Yen, H., 2014. Curie point depth from spectral analysis of magnetic data in Taiwan. J. Asian Earth Sci. 90, 26–33.
Jarrige, J., Estevou, P., Burollet, P., Montenat, C., Prat, P., Richert, J., Thiriet, J., 1990. The multistage tectonic evolution of the Gulf of Suez and northern Red Sea continental rift from field observations. Tectonics 9 (3), 441–465.
Korrat, I.M., Hussein, H.M., Marzouk, I., Ibrahim, E.M., Abdel-Fattah, R., Hurukawa, N., 2006. Seismicity of the northernmost part of the Red Sea (1995–1999). Acta Geophys. 54 (1), 33–49.
Kovach, R.L., 1986. Bouguer Anomaly Map of the Eastern Mediterranean, the Dead Sea Rift and Western Jordan. Report 87-9. Department of Geophysics, Stanford University and U.S. Geological Survey, Menlo Park, California, (11p).
Lachenbruch, A.H., Brewer, M.C., 1959. Dissipation of the temperature effect of drilling a well in Arctic Alaska. In: United States Geological Survey Bulletin 1083-C. pp. 73–109.
Lashin, A., 2013. A preliminary study on the potential of the geothermal resources around the Gulf of Suez, Egypt. Arab. J. Geosci. 6, 2807–2828.
Lashin, A., 2015. Geothermal resources of Egypt, country update. In: Proceedings World Geothermal Congress, Melbourne, Australia, (13p).
Lund, J.W., Boyd, T.L., 2015. Direct utilization of geothermal energy 2015 worldwide review. Geothermics 60, 66–93.
Martinez, F., Cochran, J., 1989. Geothermal measurements in the northern red sea, implications for lithospheric thermal structure and mode of extension during continental rifting. J. Geophys. Res. 94 (B9), 12239–12265.
Meshref, W.M., 1990. Tectonic framework of Egypt. In: Said, R. (Ed.), The Geology of Egypt. Balkema, Rotterdam, pp. 133–155.
Mohamed, H.S., Abdel-Zaher, M., Senosy, M.M., Saibi, H., El-Nouby, M., Fairhead, J.D., 2015. Correlation of aerogravity and BHT data to develop a geothermal gradient map of the northern western desert of Egypt using an artificial neural network. Pure Appl. Geophys. 172 (6), 1585–1597.
Morgan, P., Boulos, K., Swanberg, C.A., 1983. Regional geothermal exploration in Egypt. In: Geophysical Prospecting. 31, EAEG, pp. 361–376, (2).
Morgan, P., Boulos, F.K., Hennin, S.F., El-Sherif', A.A., El-Sayed, A.A., Basta, N.Z., Melek, Y.S., 1985. Heat flow in eastern Egypt, the thermal signature of a continental breakup. J. Geodyn. 4, 107–131.
Noorollahi, Y., Itoi, R., Fujii, H., Tanaka, T., 2007. GIS model for geothermal resource exploration in Akita and Iwate prefectures, northern Japan. Comput. Geosci. 33, 1008–1021.
Noorollahi, Y., Itoi, R., Fujii, H., Tanaka, T., 2008. GIS integration model for geothermal exploration and well siting. Geothermics 37, 107–131.
Nwankwo, C.N., Ekine, A.S., 2009. Geothermal gradient in the Chad Basin, Nigeria, from bottom hole temperature logs. Int. J. Phys. Sci. 4 (12), 777–783.
Okubo, Y., Graf, R.J., Hansen, R.O., Ogawa, K., Tsu, H., 1985. Curie point depths of the island of Kyushu and surrounding area Japan. Geophysics 50 (3), 481–489.
Riad, S., 1977. Shear zones in the North Egypt, interpreted from gravity data. Geophysics 42 (6), 1207–1214.
Swanberg, C.A., Morgan, E., Boulos, F.K., 1983. Geothermal potential of Egypt. Tectonophysics 96, 77–94.
Tanaka, A., Okubo, Y., Matsubayashi, O., 1999. Curie point depth based on spectrum analysis of the magnetic anomaly data in East and Southeast Asia. Tectonophysics 306 (3–4), 461–470.
Trumpy, E., Donato, A., Gianelli, G., Gola, G., Minissale, A., Montanari, D., Santilano, A., Manzella, A., 2015. Data integration and favourability maps for exploring geothermal systems in Sicily, southern Italy. Geothermics 56, 1–16.
Trumpy, E., Botteghi, S., Caiozzi, F., Donato, A., Gola, G., Montanari, D., Pluymaekers, M.P.D., Santilano, A., van Wees, J.D., Manzella, A., 2016. Geothermal potential assessment for a low carbon strategy: a new systematic approach applied in southern Italy. Energy 103, 167–181.
Waples, D.W., Ramly, M., 2001. A statistical method for correcting log-derived temperatures. Pet. Geosci. 7 (3), 231–240.
Waples, D.W., Pacheco, J., Vera, A., 2004. A method for correcting log-derived temperatures in deep wells, calibrated in the Gulf of Mexico. Pet. Geosci. 10 (3), 239–245.
Yousefi, H., Noorollahi, Y., Ehara, S., Itoi, R., Yousefi, A., Fujimitsu, Y., Nishijima, J., Sasaki, K., 2010. Developing the geothermal resources map of Iran. Geothermics 39, 140–151.